Journal of Materials Chemistry C

ROYAL SOCIETY OF CHEMISTRY

COMMUNICATION

View Article Online
View Journal | View Issue

Cite this: *J. Mater. Chem. C*, 2021, **9**, 456

Received 11th November 2020,
Accepted 30th November 2020

DOI: 10.1039/d0tc05301e

rsc.li/materials-c

Enhanced 1.54 μm luminescence of a perfluorinated erbium complex sensitized by perfluorinated Pt(II) and Zn(II) phthalocyanines with 980 nm emission†

Hongfei Li,*[ab] Xiaoqi Liu,[a] Chen Lyu,[a] Feng Ma,[c] Huanqing Ye,[a] Peter. B. Wyatt[d] and William P. Gillin[a]

By the sensitization effect of metallophthalocyanines showing ~980 nm emission to an erbium complex, a remarkably long average lifetime of 1.05 ms and an optimal PLQY of 13% with a sensitization efficiency of 81 for the Er^{3+} 1.54 μm emission are obtained in a perfluorinated organic erbium co-doped system.

Introduction

The erbium-doped optical fiber amplifier (EDFA) was reported in 1987 as an important invention for global fiber-optic telecommunication.[1] Since then, research on Er^{3+} doped waveguide amplifiers (EDWA) operating at 1.5 μm has attracted considerable attention[2–8] because multiple optical elements can be integrated on compact photonic chips to achieve optical amplification. Er^{3+} ions have weak optical absorption coefficients originating from 4f–4f electronic transitions forbidden by the Laporte rule.[3] Combining Er^{3+} ions with organic ligands can significantly enhance the near infrared (NIR) emission because the indirect excitation of Er^{3+} ions can occur by energy transfer (ET) from organic ligands *via* an antenna effect or sensitization effect.[9–13] However, chemical bonds containing H atoms such as C–H and O–H in most organic components can cause severe vibrational quenching of the 1.54 μm emission, resulting in a weak NIR emission and short lifetimes with tens of microseconds and consequently preventing Er^{3+} ions from attaining population inversion.[14–17] One effective strategy to eliminate C–H bonds is to fully fluorinate organic compounds to reduce the vibrational quenching.[18–22] The sensitized Er^{3+} energy levels of the fully fluorinated Er^{3+} complexes centre on the $^2H_{11/2}$, $^4F_{7/2}$, and $^4S_{3/2}$ energy levels, corresponding to photons of green light.[8,22,23] Such a sensitization of tris[tetrakis(pentafluorophenyl)imidodiphosphinate] Er^{3+} ($Er(F\text{-}TPIP)_3$)[18] occurs in the green region regardless of whether a 266 nm laser is used to excite $Er(F\text{-}TPIP)_3$ with sensitizing of Er^{3+} ions or the perfluorinated zinc complex $Zn(F\text{-}BTZ)_2$ or a six-coordinate iridium complex (Ir-tBuPBI) excited at 405 nm to sensitize the Er^{3+} ions in $Er(F\text{-}TPIP)_3$.[8,23] There are large energy differences between the sensitized energy levels (~2.38 eV) and the $^4I_{13/2}$ energy level (~0.81 eV) in the NIR region, and consequently, part of the energy is lost in the form of heat during the process of relaxation preceding NIR emission, leading to a decreased sensitization efficiency. Finding a sensitizer with luminescence close to the $^4I_{13/2}$ state can increase the sensitization efficiency because of the corresponding shift to a longer wavelength, and for a given photon flux, lower exciton energy means lower exciton power density (which is equal to the product of photon-flux and photon energy). With one exciton sensitizing one Er ion numerically, this approach can reduce the power needed to induce population inversion.

Phthalocyanines (Pcs) have highly delocalized 18 π-electron conjugated rings leading to extreme stability,[24,25] bright photoluminescence (PL),[26] and electroluminescence (EL) properties in the NIR region.[27,28] Metallophthalocyanines (MPcs) have contributed greatly in many fields, for example, organic dye-sensitized solar cells[29] and as photosensitizers in photodynamic therapy.[30,31] However, no available perfluorinated matrix material that can avoid self-quenching of ErPc is known. In this article, we demonstrate enhanced 1.54 μm luminescence of Er^{3+} in $Er(F\text{-}TPIP)_3$ by using M(II) hexadecafluorophthalocyanines ($F_{16}MPc$; M = Zn, Pt) as sensitizers. Both these compounds

[a] *Materials Research Institute and School of Physics and Astronomy, Queen Mary University of London, Mile End Road, London E1 4NS, UK. E-mail: h.ye@qmul.ac.uk, w.gillin@qmul.ac.ul*
[b] *State Key Laboratory on Integrated Optoelectronics, College of Electronic Science and Engineering, Jilin University, 2699 Qianjin Street, Changchun, 130012, P. R. China*
[c] *Tianjin Key Laboratory of Organic Solar Cells and Photochemical Conversion, School of Chemistry and Chemical Engineering, Tianjin University of Technology, Tianjin 300384, P. R. China*
[d] *Materials Research Institute and School of Biological and Chemical Sciences, Queen Mary University of London, Mile End Road, E1 4NS, UK. E-mail: p.b.wyatt@qmul.ac.uk*

† Electronic supplementary information (ESI) available. See DOI: 10.1039/d0tc05301e

possess luminescence at ~980 nm: F_{16}PtPc exhibits dominant phosphorescence, and the wavelength is consistent with the 980 nm excitation used for EDFA, providing high pump rate efficiency. Er(F-TPIP)$_3$ and F_{16}MPc are co-doped at the molecular level using a co-evaporation technique. Photoexcitation gives optimized sensitization efficiencies of 36 and 81 for the Er^{3+} 1.5 μm emission with F_{16}ZnPc and F_{16}PtPc, respectively. The average lifetimes for the Er^{3+} 1.5 μm emission are ~0.89 ± 0.011 ms (doped with F_{16}ZnPc) and ~1.04 ± 0.012 ms (doped with F_{16}PtPc). This is so far the longest lifetime of organic sensitized Er^{3+} 1.5 μm emission, which can even match those of the inorganic systems.[32] A maximum photoluminescence quantum yield (PLQY) of 13% is obtained for the sensitized Er^{3+} 1.5 μm emission in an organic co-doped system.

Results and discussion

The chemical structures of F_{16}MPc and Er(F-TPIP)$_3$ are depicted in Fig. 1. F_{16}PtPc was synthesized and purified by modifying a published procedure for the preparation of F_{16}CuPc.[33] F_{16}PtPc of good purity was obtained following a simple reprecipitation from 98% sulfuric acid by dilution with water. This approach avoids the need for preparative chromatography, which can be difficult to scale up for Pc derivatives due to their generally low solubility in organic solvents. The purity and identity of F_{16}PtPc were confirmed by MALDI-TOF mass spectrometry, as shown in Fig. S1 (ESI†). The most intense peak (m/z 996) corresponded to the protonation of F_{16}PtPc by the MALDI matrix and aromatic carboxylic acids to form an $[F_{16}PtPc + H]^+$ pseudo molecular ion containing the abundant ^{195}Pt nuclide. This was part of an isotopic cluster, as expected, based on the natural occurrence of other stable isotopes. There were no detectable impurities, apart from a group of very weak peaks, 16 atomic mass units heavier than the main cluster; these had an intensity <1% of the major component and were attributed to halogen exchange with platinum(II) chloride having occurred during the Pc ring synthesis, forming traces of ClF_{15}PtPc. The ^{19}F NMR spectrum of F_{16}PtPc in D_2SO_4 solution showed just two aromatic fluorine environments: these had equal integrals, which is consistent with the expected four-fold symmetry of the highly delocalised phthalocyanine system. The energy dispersive X-ray (EDS) spectrum shown in Fig. S2 (ESI†) confirmed the presence of C, N, F, and Pt; Cl is too weak to be detected. The successful synthesis of F_{16}PtPc was also supported by Fourier transform infrared (FTIR) spectroscopy. As shown in Fig. S3 (ESI†), the synthesized F_{16}PtPc has seven groups of peaks similar to the IR spectrum of F_{16}CuPc,[34] consistent with the successful formation and metalation of the F_{16}Pc macrocycle.

Since the F_{16}MPcs have a large coplanar conjugated system of 18 π electrons, they could form molecular aggregates and quench the luminescence, which would disfavor energy transfer from F_{16}MPc to Er(F-TPIP)$_3$.[35] Absorption spectra provide a method to study the aggregation. As shown in Fig. 2a, the electronic absorption spectra of F_{16}ZnPc in acetone solution and in a film deposited onto a glass substrate show two distinct

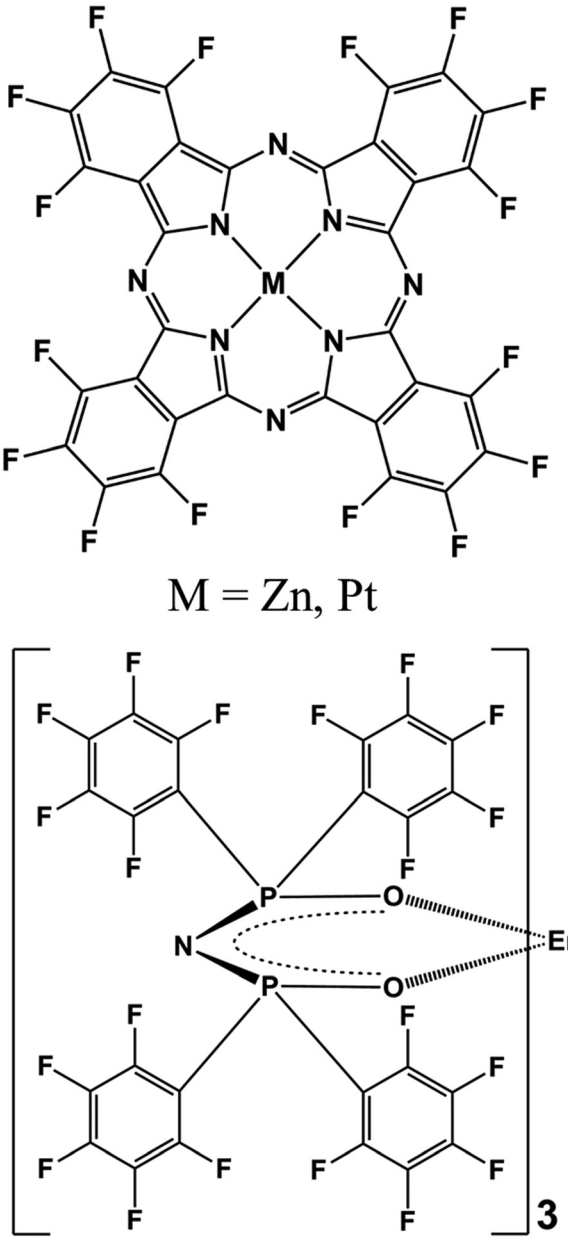

Fig. 1 The chemical structures of F_{16}MPc and Er(F-TPIP)$_3$.

absorption bands from the UV to the NIR spectral region. The high-energy absorption band in the region of <450 nm is ascribed to the B-band originating from a direct electronic transition from a_{2u} orbital to e_g orbital. The low energy absorption band in the region from 500 to 850 nm is ascribed as a Q-band originating from an a_{1u} to e_g transition. The Q band of the F_{16}ZnPc solution in acetone shows two absorption bands at 635 and 667 nm with a shoulder at 580 nm that indicates the dimer behavior of F_{16}ZnPc in solution.[34] In comparison, it is found that the spectrum of a neat F_{16}ZnPc film shows both significant broadening and a bathochromic shift; these are typical effects of aggregation behavior.[36] However, the absorption spectrum of the Q band of F_{16}ZnPc in a 50% Er(F-TPIP)$_3$:50% F_{16}ZnPc co-doped film appears as one band at 624 nm with a weak shoulder

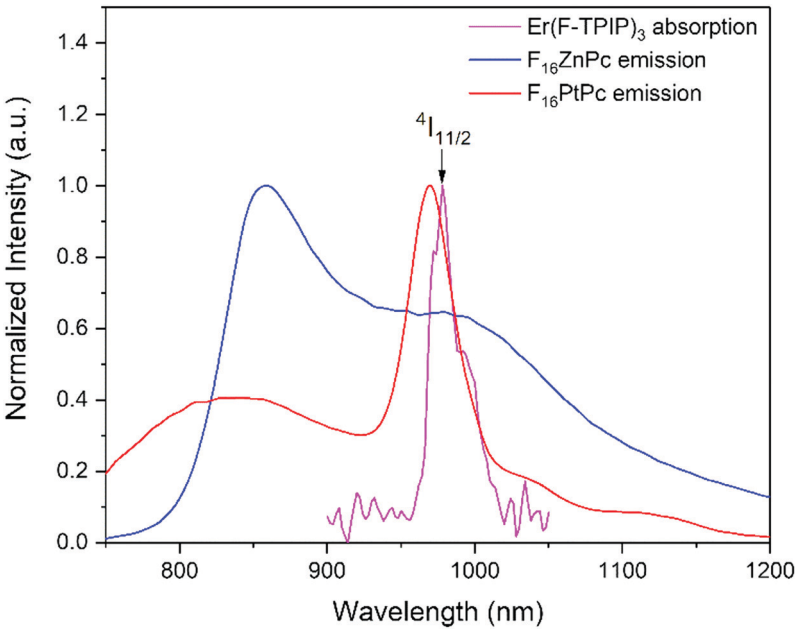

Fig. 2 The absorption spectra of (a) F_{16}ZnPc and (b) F_{16}PtPc. (A) Dissolved in acetone. (B) Neat film. (C) Co-doped film with 50% Er(F-TPIP)$_3$.

at 675 nm. Compared to that of neat F_{16}ZnPc film, this absorption band is dramatically narrowed and its full width at half maximum (FWHM) is only slightly wider than that in solution. The comparison indicates that the aggregation of the F_{16}ZnPc molecules in the co-doped film is effectively suppressed, and they are likely to be dispersed homogeneously.

The Q band of F_{16}PtPc in the solution, neat and co-doped films are similar, and the FWHM of the Q band of the 50% Er(F-TPIP)$_3$:50% F_{16}PtPc co-doped film is even slightly narrower than that in solution (Fig. 2b). This contrasts markedly with F_{16}ZnPc (Fig. 2a) considered above, where the Q band of F_{16}ZnPc in the neat film is significantly different from those in the solution and the co-doped film. Especially, F_{16}PtPc in the co-doped film shows one Q band, which indicates that the F_{16}PtPc molecules in the co-doped film exist homogeneously as monomers.

The emission spectra of neat F_{16}ZnPc and F_{16}PtPc films are shown in Fig. 3. Zn^{2+} has a relatively low atomic number and a d^{10} closed shell structure without any unpaired electrons, leading to a low probability of intersystem crossing (ISC).[37] Its very weak phosphorescence possibly comes from the $\pi \rightarrow \pi^*$ transition of the F_{16}Pc ligands. Because no long-lived emission is detected at room temperature, we can attribute the luminescence of F_{16}ZnPc at about 980 nm to fluorescence. On the other hand, non-fluorinated PtPc exhibits phosphorescence in the NIR region, and the perfluorination of PtPc can further increase the ISC, so F_{16}PtPc is regarded as a phosphorescent material.[38–40]

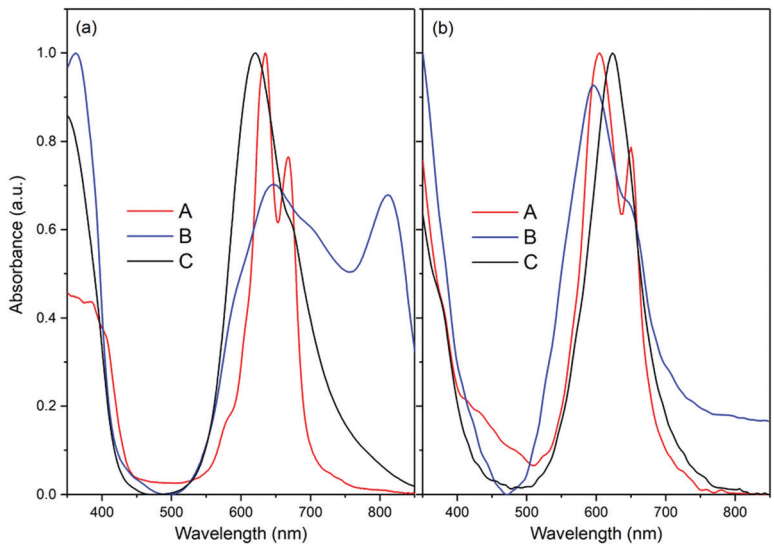

Fig. 3 Absorption spectrum of $^4I_{15/2} \rightarrow {}^4I_{11/2}$ of Er^{3+} ion in an Er(F-TPIP)$_3$ crystal; emission spectra of neat F_{16}ZnPc and F_{16}PtPc films.

Table 1 Calculated emission energies (eV), oscillator strength (f) and radiative lifetime τ (s) by SOC-TDDFT at PBE/TZ2P level of theory

State	ΔE [eV]	λ [nm]	f	Transition contribution	Assignment	T [s]
$^3A_{1u}$	1.3173	941.3	0.000	$61e_{1/2g} \rightarrow 61e_{1/2u}$ (0.9986)	^{3}LC/^{3}MLCT	—
$^3A_{2u}$	1.3173	941.3	0.2438×10^{-7}	$61e_{1/2g} \rightarrow 61e_{1/2u}$ (0.9986)	^{3}LC/^{3}MLCT	0.5447
^3E_u	1.3346	929.1	0.1015×10^{-3}	$61e_{1/2g} \rightarrow 61e_{1/2u}$ (0.5199)	^{3}LC/^{3}MLCT	1.275×10^{-4}
^3E_u	1.3346	929.1	0.1015×10^{-3}	$58e_{3/2g} \rightarrow 61e_{1/2u}$ (0.4789)	^{3}LC/^{3}MLCT	1.275×10^{-4}
$^3B_{1u}$	1.3519	917.2	0.000	$61e_{1/2g} \rightarrow 61e_{1/2u}$ (0.9987)	^{3}LC/^{3}MLCT	—
$^3B_{2u}$	1.3519	917.2	0.000	$58e_{3/2g} \rightarrow 61e_{1/2u}$ (0.9987)	^{3}LC/^{3}MLCT	—

To gain insight into the origin of the intense emission peak at *ca.* 980 nm of the neat F_{16}PtPc film, we have performed SOC-TDDFT calculations based on the T_1 excited state structure. The calculated emission energies in terms of wavelength and dominant orbital transitions for the low-lying triplet excited states are collected in Table 1, and the important frontier molecular orbitals are shown in Fig. 4. The calculated emission wavelength in the Franck–Condon state (T_1 equilibrium geometry) for F_{16}PtPc is 940 nm, which relates well to the experimental phosphorescence peak of 980 nm. As shown in Table 1, the lowest energy transitions for these emission bands are LUMO → HOMO transitions. From Fig. 4, the LUMO ($61e_{1/2g}$) is largely a π orbital of F_{16}Pc mixed with the dπ of Pt, and the HOMO ($61e_{1/2u}$) is largely a π* orbital on the F_{16}Pc. We attribute the origin of the 980 nm emission in the experiment to mixed metal-to-ligand charge transfer (^{3}MLCT) and ligand-centered (^{3}LC) characteristics. The calculated long excited-state lifetime of 544.7 μs confirms that F_{16}PtPc emits phosphorescence.

The absorption spectrum of the Er^{3+} ion in the Er(F-TPIP)$_3$ crystal in the NIR region is shown in Fig. 3. Both the broad emission bands of F_{16}ZnPc and especially F_{16}PtPc have good overlap of the absorption band of $^4I_{15/2} \rightarrow {}^4I_{11/2}$ of the Er^{3+} ion in Er(F-TPIP)$_3$, which means that an efficient sensitization may be realized through energy transfer from F_{16}MPc to Er(F-TPIP)$_3$.

In order to study the sensitization effect of F_{16}ZnPc on Er(F-TPIP)$_3$, a series of Er(F-TPIP)$_3$:F_{16}ZnPc co-doped films with the concentrations of Er(F-TPIP)$_3$ varying from 20% to 80% were prepared; their emission spectra are shown in Fig. 5a. It is found that the emission intensity of F_{16}ZnPc at ∼980 nm tends to decrease with increasing Er(F-TPIP)$_3$ concentration, implying that energy is transferred to Er(F-TPIP)$_3$ quenching the excitation of F_{16}ZnPc. The emission spectra of the Er(F-TPIP)$_3$:F_{16}PtPc co-doped films under the excitation of a 655 nm laser are shown in Fig. 5b. It is found that the centre of the emission spectrum is shifted from 970 nm in the neat F_{16}PtPc film to ∼980 nm in the co-doped film. Being different from the Er(F-TPIP)$_3$:F_{16}ZnPc co-doped films, the dips in the mixed ^{3}LC/^{3}MLCT emission spectra of F_{16}PtPc in co-doped films appeared at ∼980 nm, which was not found in the spectrum of the neat F_{16}PtPc film as shown in Fig. 3. Their shapes resemble those of the inverted absorption bands of Er(F-TPIP)$_3$ at ∼980 nm, as shown in Fig. 5b. This is a clear evidence that there is an energy transfer mechanism based on the emission–reabsorption process where the Er^{3+} $^4I_{11/2}$ state absorbs part of the F_{16}PtPc emission.[41,42] This mechanism is different from the Förster energy transfer, wherein the whole emission intensity of F_{16}PtPc should be decreased with no change in spectral features.

It is interesting that there is no dip in the emission spectrum of F_{16}PtPc in the 20% Er(F-TPIP)$_3$:80% F_{16}PtPc co-doped film. This means that the re-absorption process does not occur at this concentration, and there may be another energy transfer path from F_{16}PtPc to Er(F-TPIP)$_3$. Förster transfer is a resonant dipole coupling process that is dependent on the overlap between the donor emission spectrum and the acceptor absorption spectrum. Here the overlap between the PL spectrum of F_{16}PtPc and the absorption of Er(F-TPIP)$_3$ is obvious, as shown in Fig. 3. It indicates that the Förster energy transfer may also be an efficient mechanism and suggests that the energy transfer process from F_{16}PtPc to Er(F-TPIP)$_3$ comprises Förster transfer and emission–reabsorption. The energy transfer paths are shown in Fig. 6. The 20% Er(F-TPIP)$_3$:80% F_{16}PtPc co-doped film shows

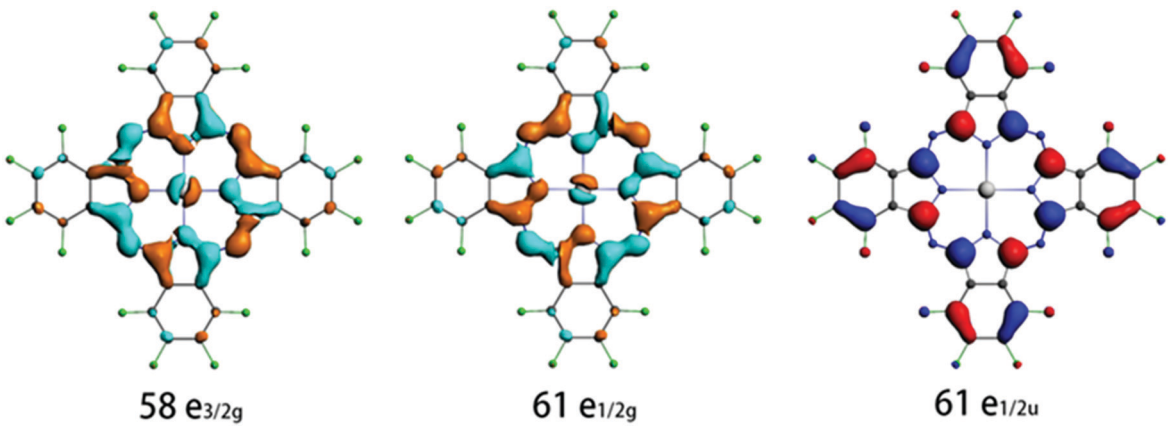

Fig. 4 Calculated electronic density contours of the frontier molecular orbitals involved in the main electronic transitions.

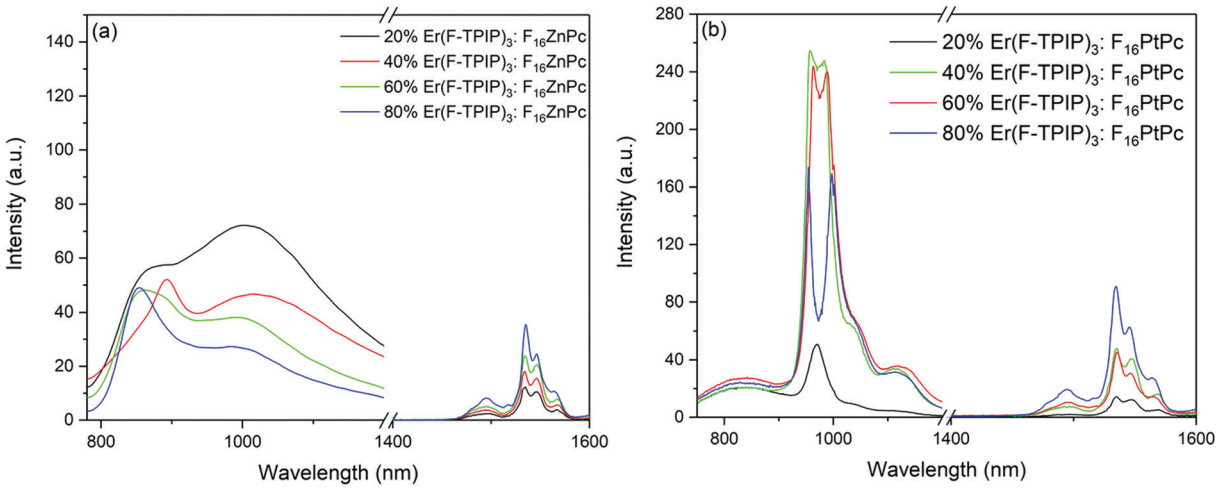

Fig. 5 Emission spectra of (a) Er(F-TPIP)$_3$:F$_{16}$ZnPc and (b) Er(F-TPIP)$_3$:F$_{16}$PtPc co-doped films with different Er(F-TPIP)$_3$ concentrations. λ_{ex} = 655 nm.

the weakest 1.54 μm emission from Er(F-TPIP)$_3$ due to the low concentration of Er(F-TPIP)$_3$. Meanwhile, given the weak emission from F$_{16}$PtPc, there could be a triplet–triplet annihilation (TTA) due to highly concentrated 80% F$_{16}$PtPc, which reduces the energy transfer. As the concentration of Er(F-TPIP)$_3$ is increased, the 1.54 μm emission of Er(F-TPIP)$_3$ increases gradually while the emission of F$_{16}$PtPc decreases. The strongest 1.54 μm emission is obtained based on 80% Er(F-TPIP)$_3$ doped concentration, due to the increase in the Er(F-TPIP)$_3$ molecules and possibly a decrease in the TTA effect in F$_{16}$PtPc.

To quantify the sensitization efficiency, the Er(F-TPIP)$_3$:Y(F-TPIP)$_3$ co-doped films with different diluted Er^{3+} concentrations were used as reference samples, where Y^{3+} is optically inactive, resulting in the exclusion of energy transfer from Y(F-TPIP)$_3$ to Er(F-TPIP)$_3$. The measurement set up is identical for all co-doped films. The power-dependent Er^{3+} PL intensities of these co-doped films with Er^{3+} concentrations of 20%, 40%, 60%, and 80% recorded at 1532 nm are shown in Fig. 7, where the Er^{3+} ions are directly excited to the $^4F_{9/2}$ level. In the co-doped films containing the sensitizers, 655 nm photoexcitation of F$_{16}$ZnPc and F$_{16}$PtPc was again used to induce sensitization. Hence, the 1532 nm emission intensities from both the F$_{16}$ZnPc and F$_{16}$PtPc co-doped films are larger than those of the Y(F-TPIP)$_3$ doped films. The sensitization effect can be simply calculated by fitting the emission intensity of the Y(F-TPIP)$_3$ doped films *versus* power density, which shows a linear correlation. Subsequently, the power densities used in F$_{16}$MPc can be used in the correlation to calculate the corresponding 1532 nm emission intensity, and these values can be used to divide the measured 1532 nm intensity to get the sensitization efficiency. The values of the sensitization efficiency for F$_{16}$ZnPc/F$_{16}$PtPc in different Er(F-TPIP)$_3$ doped films are listed in Table 2. The sensitization efficiency decreased with the increased percentage of Er(F-TPIP)$_3$ in the F$_{16}$ZnPc doped films. F$_{16}$PtPc behaves differently, the reason being that the TTA effect of F$_{16}$PtPc is quite strong. However, under a high concentration of Er(F-TPIP)$_3$, the F$_{16}$PtPc molecules get separated and the TTA effect is dramatically decreased, and the emission from F$_{16}$PtPc gets stronger so that more energy can be transferred to the Er^{3+} ions through the re-absorption effect. In addition, long-lived triplet excitons of F$_{16}$PtPc travel over a long distance to sensitize Er^{3+} ions, along with the perfect overlap between the absorption band of Er(F-TPIP)$_3$ and the emission peak of F$_{16}$PtPc. So, F$_{16}$PtPc shows a more efficient sensitization effect than F$_{16}$ZnPc with high Er(F-TPIP)$_3$ doped concentration.

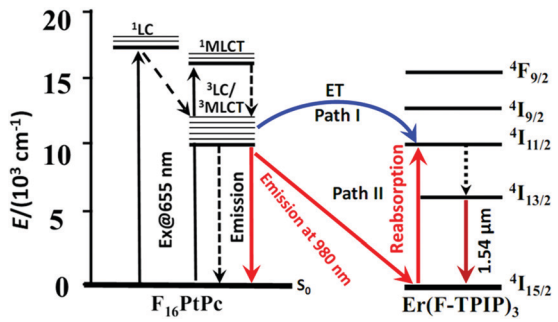

Fig. 6 Schematic energy diagram describing the two sensitization mechanisms of NIR luminescence of Er(F-TPIP)$_3$ *via* F$_{16}$PtPc energy transfer (path I) and emission–reabsorption (path II).

The time-resolved PL (TRPL) decay curves for the F$_{16}$PtPc emission recorded at 980 nm with different Er(F-TPIP)$_3$ doped concentration films are shown in Fig. 8a. The values of their short component (τ_S), long component (τ_L), and average lifetimes (τ_{Ave}) are listed in Table 3a. The lifetime of the F$_{16}$ZnPc is too short to be measured, lying below the detection limit of the equipment ($\sim$5 ns) due to the strong self-quenching. In F$_{16}$PtPc doped films, the changing concentrations affect the τ_L of F$_{16}$PtPc through two opposing processes: (I) with increased Er(F-TPIP)$_3$ concentrations, F$_{16}$PtPc is diluted, and the reduced TTA effect leads to increased τ_L. (II) At the same time, each F$_{16}$PtPc molecule is surrounded by more Er(F-TPIP)$_3$ molecules; their excitons can more easily transfer their energy to the central Er^{3+} ions in Er(F-TPIP)$_3$, thus tending to reduce τ_L. As the Er(F-TPIP)$_3$ concentration increases from 20% to 60%, τ_L gradually increases from 1.00 $\pm$ 0.015 ms to 1.89 $\pm$ 0.017 ms

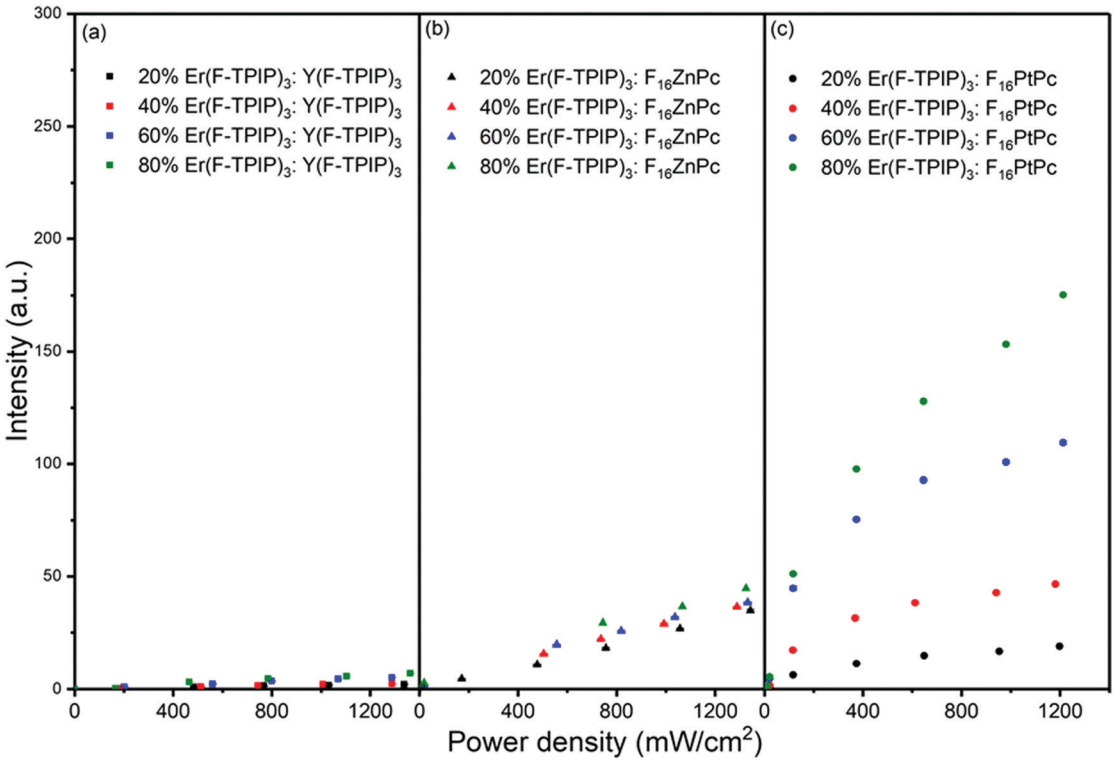

Fig. 7 The emission intensity at 1532 nm as a function of laser power density for co-doped films with different Er(F-TPIP)$_3$ concentrations diluted by (a) Y(F-TPIP)$_3$, (b) F_{16}ZnPc, and (c) F_{16}PtPc, respectively. λ_{ex} = 655 nm.

Table 2 The sensitization efficiency of F_{16}ZnPc and F_{16}PtPc in co-doped films with different concentrations of Er(F-TPIP)$_3$

Sample	Concentration [%]	Sensitization efficiency
Er(F-TPIP)$_3$:F_{16}ZnPc	20	36 ± 1.6
Er(F-TPIP)$_3$:F_{16}ZnPc	40	32 ± 1.3
Er(F-TPIP)$_3$:F_{16}ZnPc	60	30 ± 1.2
Er(F-TPIP)$_3$:F_{16}ZnPc	80	28 ± 1.2
Er(F-TPIP)$_3$:F_{16}PtPc	20	22 ± 1.1
Er(F-TPIP)$_3$:F_{16}PtPc	40	53 ± 2.3
Er(F-TPIP)$_3$:F_{16}PtPc	60	70 ± 3.2
Er(F-TPIP)$_3$:F_{16}PtPc	80	81 ± 3.9

because factor (I) plays the dominant role. However, in the 80% Er(F-TPIP)$_3$ doped film, τ_L decreases to 1.30 ± 0.014 ms as factor (II) is predominant. Basically, the energy transfer from F_{16}PtPc to Er(F-TPIP)$_3$ is more efficient with an increase in Er(F-TPIP)$_3$ because more energy is transferred to Er(F-TPIP)$_3$, which causes the lifetime of F_{16}PtPc to decrease from 484.64 ± 7.09 μs to 384.48 ± 6.39 when the Er(F-TPIP)$_3$ concentration is increased from 20% to 80%.

The results of TRPL measurements for the Er^{3+} emission lifetimes (λ_{mon} = 1532 nm) with different concentrations of Er(F-TPIP)$_3$ films doped with F_{16}ZnPc and F_{16}PtPc are shown in Fig. 8b, c and Table 3b and c, respectively. The decay can be described by a biexponential process, with two lifetime components for Er^{3+} in each co-doped film. Being sensitized by F_{16}ZnPc and F_{16}PtPc, the rise in the Er(F-TPIP)$_3$ concentrations makes their τ_S and τ_L to increase, which shows the same trend of the emission intensity of Er(F-TPIP)$_3$ as shown in Fig. 5, except for the 80% Er(F-TPIP)$_3$:F_{16}PtPc co-doped film. Compared to the 60% Er(F-TPIP)$_3$ doped film, the τ_L of the 80% Er(F-TPIP)$_3$ doped film is slightly decreased. With the increase in Er(F-TPIP)$_3$ doped concentration, although their τ_S and τ_L are increased, the erbium ion–ion interaction is also increased. This leads the percentage contribution of τ_L to be reduced, while τ_S is increased, which makes τ_{Ave} almost unaffected by the doped concentrations of sensitizers. τ_S and τ_{Ave} of Er^{3+} in the F_{16}PtPc co-doped films are longer than those of the F_{16}ZnPc co-doped films because of the long phosphorescence lifetimes of F_{16}PtPc and the emission–reabsorption process from F_{16}PtPc to Er(F-TPIP)$_3$ in doped films. The longest average lifetime of 0.91 ± 0.015 and 1.05 ± 0.041 ms for F_{16}ZnPc and F_{16}PtPc co-doped films are obtained, and they are 4.55 and 5.25 times longer than the neat Er(F-TPIP)$_3$ film (0.2 ms), respectively. This prolonged Er^{3+} lifetime is caused by the long-lived organic triplet excitons;[43] so the largest PLQY of 13% is achieved in the F_{16}PtPc co-doped film, which is the highest ever reported for erbium in an organic complex.

Conclusions

We demonstrate that two fully fluorinated MPcs: F_{16}ZnPc and F_{16}PtPc can be used as sensitizers to enhance the Er 1.54 μm emission in the co-doped organic Er^{3+} complex systems. This significantly reduces the energy difference between the sensitized Er^{3+} energy levels and the $^4I_{13/2}$ level by utilizing perfluorinated 980 nm luminescent chromophores and consequently decreases the energy loss caused by the Er^{3+} nonradiative transitions from the

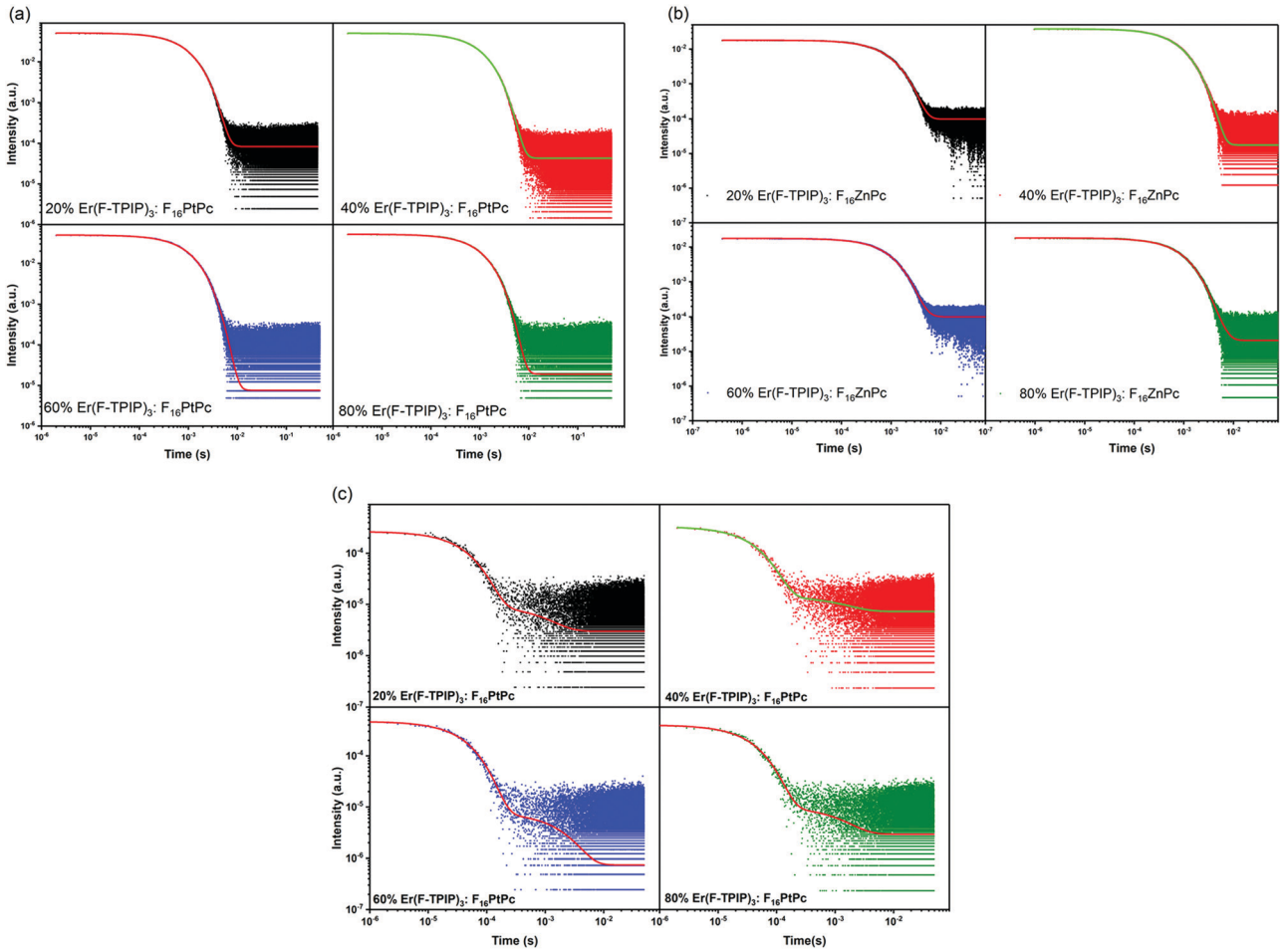

Fig. 8 (a) The TRPL decay of the F_{16}PtPc doped films with Er(F-TPIP)$_3$ concentration varying from 20% to 80%. λ_{mon} = 980 nm. The TRPL decay of Er(F-TPIP)$_3$ in (b) F_{16}ZnPc doped films and (c) F_{16}PtPc doped films. λ_{mon} = 1532 nm.

higher sensitized energy levels to the $^4I_{13/2}$ level. Optimized sensitization efficiencies of 36 and 81 are obtained for the Er^{3+} complex doped with F_{16}ZnPc and F_{16}PtPc, respectively. An average lifetime for the Er^{3+} 1.5 μm emission in an Er(F-TPIP)$_3$–F_{16}PtPc system reaches ~1 ms, which is by far the longest ever reported. 13% PLQY is achieved in the F_{16}PtPc doped film that is the highest ever reported for erbium in an organic system. Our research opens the door for improving power efficiency to reach population inversion of Er ions based on the perfluorinated organic system.

Experimental

Chemical reagents

F_{16}ZnPc (90%) was purchased from Sigma Aldrich and purified by sublimation under 280 °C at a pressure of ~5 × 10^{-6} mbar. 3,4,5,6-Tetrafluorophthalo-1,2-dinitrile and anhydrous platinum(II) chloride were obtained from Energy Chemical and Mascal companies, respectively.

Synthesis of F_{16}PtPc

3,4,5,6-Tetrafluorophthalo-1,2-dinitrile (0.40 g, 2 mmol) and anhydrous platinum(II) chloride (0.13 g, 0.5 mmol) were mixed well and placed in a glass vessel. The vessel was sealed under vacuum (0.13 Pa) and then slowly heated to 210 °C for 6 hours. After cooling to room temperature, the crude purple product was isolated and washed with petroleum ether and ethanol. The crude F_{16}PtPc product was dissolved in concentrated sulfuric acid (~2 ml) with intense stirring in an ice-water bath for 1 hour at a solution temperature not exceeding 5 °C. Then it was filtered by a sintered glass filter, and the filtrate was slowly added to the ice water mixture under stirring and at a temperature lower than 10 °C. Finally, the suspension was filtered and the cake was washed to neutral with deionized water. After drying, the F_{16}PtPc product (0.21 g, 43%) was obtained as a purple solid. ^{19}F NMR (377 MHz, D_2SO_4 solution) δ_F: −129.6 (8F, br s) and −137.2 (8F, br s); IR (KBr, cm^{-1}): C–F (1496 s), C=C (1530 s), C=N (1647 w), Pc ring (750 w, 1160 s and 1469 s), N–Pt–N (845 w). UV/Vis: λ_{max} = 605 nm. MS (MALDI-TOF): *m*/*z* calcd for $[M + H]^+$ $[C_{32}HF_{16}N_8{}^{195}Pt]^+$, 996.0; found: 996.1.

Theoretical calculations

All calculations were performed with the ADF 2013.01 program package.[44] The geometry optimization of the ground state (S_0) and lowest triplet excited state (T_1) was carried out using gradient

Table 3 (a) The lifetime components and average lifetime of F_{16}PtPc emission (λ_{mon} = 980 nm) in the Er(F-TPIP)$_3$:F_{16}PtPc co-doped films with different F_{16}PtPc concentrations. (b) The Er^{3+} 1.5 μm emission lifetime components and average lifetimes in the Er(F-TPIP)$_3$:F_{16}ZnPc co-doped films with different F_{16}ZnPc concentrations. (c) The Er^{3+} 1.5 μm emission lifetime components and average lifetimes in the Er(F-TPIP)$_3$:F_{16}PtPc co-doped films with different Er(F-TPIP)$_3$ concentrations

(a)

Concentration [%]	τ_S [μs]	τ_L [ms]	τ_{Ave} [μs]
20	43.50 ± 0.047 (64%)	1.30 ± 0.014 (36%)	484.64 ± 7.09
40	45.75 ± 0.039 (61%)	1.89 ± 0.017 (39%)	754.29 ± 7.00
60	43.44 ± 0.068 (52%)	1.45 ± 0.010 (48%)	708.62 ± 8.56
80	44.89 ± 0.076 (64%)	1.00 ± 0.015 (36%)	384.48 ± 6.39

(b)

F_{16}ZnPc concentrations [%]	Short component τ_S [ms]	Long component τ_L [ms]	Average lifetime τ_{Ave} [ms]
80	0.67 ± 0.0025 (49%)	1.08 ± 0.0047 (51%)	0.88 ± 0.015
60	0.68 ± 0.0013 (62%)	1.22 ± 0.0048 (38%)	0.89 ± 0.003
40	0.76 ± 0.0009 (81%)	1.45 ± 0.0116 (19%)	0.89 ± 0.014
20	0.77 ± 0.0006 (86%)	1.72 ± 0.0213 (14%)	0.91 ± 0.015

(c)

Er(F-TPIP)$_3$ concentrations [%]	Short component τ_S [ms]	Long component τ_L [ms]	Average lifetime τ_{Ave} [ms]
20	0.85 ± 0.0025 (48%)	1.22 ± 0.0012 (52%)	1.04 ± 0.025
40	0.90 ± 0.0013 (65%)	1.30 ± 0.0014 (35%)	1.04 ± 0.034
60	0.95 ± 0.0009 (82%)	1.50 ± 0.0016 (18%)	1.05 ± 0.041
80	0.98 ± 0.0006 (91%)	1.46 ± 0.0010 (9%)	1.02 ± 0.047

approximation (GGA) using the PBE exchange–correlation functional.[45] All electron TZ2P basis set was employed for all atoms, and the relativistic effect was also taken into account *via* the zeroth-order regular approximation (ZORA).[46,47] On the basis of the optimized T_1 geometry, relativistic calculations were performed to obtain electron excitations and radiative rate. In these calculations, spin–orbit coupling (SOC) was included in one-component time dependent density functional theory (TDDFT) utilizing the ZORA.[48,49] The radiative rate (k_r) of an excited state was then calculated as[50]

$$k_r = 2\varepsilon^2 f/c^3$$

where ε is the excitation energy and f is the corresponding oscillator strength for the electronic excitation from the ground state to the excited state.

Sample preparation

Co-doped films of Er(F-TPIP)$_3$:F_{16}MPc and Er(F-TPIP)$_3$:Y(F-TPIP)$_3$ were deposited by vacuum sublimation at a vacuum pressure of $\sim 10^{-7}$ mbar. 120 nm thick aluminium was evaporated onto the organic layer to protect the material from atmospheric degradation. Samples were prepared with Er(F-TPIP)$_3$ at a molecular concentration of 20%, 40%, 60%, and 80%. In F_{16}MPc doped films, they had an identical amount of F_{16}MPc chromophore (75 nm thick). In the Y(F-TPIP)$_3$ doped film, the thickness of Y(F-TPIP)$_3$ was kept constant as 163 nm.

Instruments and measurements

The UV-vis electronic absorption measurements were performed using a Shimadzu UV-2600 spectrophotometer. The Fourier-transform infrared (FT-IR) spectrum was collected in the range 400–4000 cm^{-1} on a Nicolet Fourier spectrophotometer using KBr pellets. The mass spectrum was measured with a MALDI-TOF/TOF Mass spectrometer, Ultraflex Treme TOF/TOF (Bruker). The analysis of chemical composition was performed on a Zeiss Merlin Compact scanning electron microscope with an energy dispersive X-ray spectrometer.

Emission spectra and TRPL measurements

For the PL measurements, lasers of different wavelengths were used to excite the samples; the emission from the samples were guided into a spectrometer (Jobin Yvon Horiba Triax 550), and the reflected laser light was removed by putting high-pass filters in front of the spectrometer. The spectrometer was connected to a photomultiplier (PMT), and the signal from the PMT was transmitted to an oscilloscope or a lock-in-amplifier for time-resolved or emission spectrum measurements, respectively. A Q-switch Nd:YAG laser was used to produce pulsed laser, and the laser wavelength was tuned by using an optical parametric oscillator (OPO). Pulsed laser beams were made to be incident on co-doped films to give TRPL data. The data were fitted by using exponential functions: $I(t) = I_0 + \sum_i A_i \exp[-t/\tau_i]$. A lifetime component percentage is obtained by an expression of $A_i\tau_i / \sum_i A_i\tau_i$. An average lifetime is obtained by an expression of $\langle\tau\rangle = \sum_i \left[\tau_i A_i \tau_i \Big/ \left(\sum_i A_i\tau_i\right)\right]$.

Sensitization measurement

Two apertures were used to ensure the consistency of the alignment of the optical path. A mirror, made by growing an

aluminium circle with 2 mm diameter on the 20 mm × 20 mm glass substrate, was set to an angle of 45° to reflect light normally onto the sample and allow the PL to be collected. An aperture with a 1 mm diameter hole was placed directly in front of the sample, and the laser was defocused to ensure uniform illumination over the whole sample. Once the optical path was set up, the measurement was started with the $Er(F\text{-}TPIP)_3$:$Y(F\text{-}TPIP)_3$ co-doped films; the 655 nm laser was used to directly excite the Er^{3+} ions, and the emission was monitored at 1532 nm. The laser power was increased from low to high. At each power, ten measurements were taken to determine the statistical errors. After measuring with the $Y(F\text{-}TPIP)_3$ doped films, the experiment was repeated using the $Er(F\text{-}TPIP)_3$:$F_{16}ZnPc$/$F_{16}PtPc$ co-doped films. After the data were collected, the sample was replaced with a calibrated silicon detector to measure the excitation power density on the sample.

Conflicts of interest

There are no conflicts to declare.

Acknowledgements

This work was supported by the China Scholarship Council, Queen Mary University of London. W. P. G. acknowledges financial support from EPSRC (EP/L020114/1 and EP/P007767/1).

References

1 R. J. Mears, L. Reekie, I. M. Jauncey and D. N. Payne, *Electron. Lett.*, 1987, **23**, 1026–1028.
2 H. S. Han, S. Y. Seo and J. H. Shin, *Appl. Phys. Lett.*, 2001, **79**, 4568–4570.
3 L. H. Sloff, A. Van Blaaderen, A. Polman, G. A. Hebbink, S. I. Klink, F. C. M. Van Veggel, D. N. Reinhoudt and J. W. Hofstraat, *J. Appl. Phys.*, 2002, **91**, 3955–3980.
4 W. H. Wong, E. Y. B. Pun and K. S. Chan, *Appl. Phys. Lett.*, 2004, **84**, 176–178.
5 A. Q. Le Quang, R. Hierle, J. Zyss, I. Ledoux and S. Pietralunga, presented at 2006 Conference on Lasers and Electro-Optics and 2006 Quantum Electronics and Laser Science Conference, Long Beach, CA, 2006.
6 S. Ghatrehsamani and G. E. Town, *IEEE J. Quantum Electron.*, 2017, **53**, 7000705.
7 X. S. Zhai, S. S. Liu, X. Y. Liu, F. Wang, D. M. Zhang, G. S. Qin and W. P. Qin, *J. Mater. Chem. C*, 2013, **1**, 1525–1530.
8 H. Q. Ye, Z. Li, Y. Peng, C. C. Wang, T. Y. Li, Y. X. Zheng, A. Sapelkin, G. Adamopoulos, I. Hernández, P. B. Wyatt and W. P. Gillin, *Nat. Mater.*, 2014, **13**, 382–386.
9 F. J. Steemers, W. Verboom, J. W. Hofstraat, F. A. J. Geurts and D. N. Reinhoudt, *Tetrahedron Lett.*, 1998, **39**, 7583–7586.
10 V. Bulach, F. Sguerra and M. W. Hosseini, *Coord. Chem. Rev.*, 2012, **256**, 1468–1478.
11 C. Y. Chow, S. V. Eliseeva, E. R. Trivedi, T. N. Nguyen, J. W. Kampf, S. Petoud and V. L. Pecoraro, *J. Am. Chem. Soc.*, 2016, **138**, 5100–5109.
12 Z. F. Li, J. B. Yu, L. Zhou, H. J. Zhang, R. P. Deng and Z. Y. Guo, *Org. Electron.*, 2008, **9**, 487–494.
13 L. N. Sun, H. J. Zhang, L. S. Fu, F. Y. Liu, Q. G. Meng, C. Y. Peng and J. B. Yu, *Adv. Funct. Mater.*, 2005, **15**, 1041–1048.
14 Y. Hasegawa, Y. J. Wada and S. Yanagida, *J. Photochem. Photobiol., C*, 2004, **5**, 183–202.
15 R. H. C. Tan, M. Motevalli, I. Abrahams, P. B. Wyatt and W. P. Gillin, *J. Phys. Chem. B*, 2006, **110**, 24476–24479.
16 L. Winkless, R. H. C. Tan, Y. Zheng, M. Motevalli, P. B. Wyatt and W. P. Gillin, *Appl. Phys. Lett.*, 2006, **89**, 111115.
17 F. Artizzu, L. Marchiò, M. Mercuri, L. Pilia, A. Serpe, F. Quochi, R. Orrù, F. Cordella, M. Saba, A. Mura, G. Bongiovanni and P. Deplano, *Adv. Funct. Mater.*, 2007, **17**, 2365–2376.
18 G. Mancino, A. J. Ferguson, A. Beeby, N. J. Long and T. S. Jones, *J. Am. Chem. Soc.*, 2005, **127**, 524–525.
19 G. A. Kumar, R. E. Riman, L. A. D. Torres and O. B. Garcia, *Chem. Mater.*, 2005, **17**, 5130–5135.
20 P. B. Glover, A. P. Bassett, P. Nockemann, B. M. Kariuki, R. V. Deun and Z. Pikramenou, *Chem. – Eur. J.*, 2007, **13**, 6308.
21 A. Monguzzi, R. Tubino, F. Meinardi, A. O. Biroli, M. Pizzotti, F. Demartin, F. Quochi, F. Cordella and M. A. Loi, *Chem. Mater.*, 2009, **21**, 128–135.
22 Y. Peng, H. Q. Ye, Z. Li, M. Motevalli, I. Hernández, W. P. Gillin and P. B. Wyatt, *J. Phys. Chem. Lett.*, 2014, **5**, 1560–1563.
23 H. F. Li, X. Q. Liu, C. Lyu, J. Gorbaciova, L. L. Wen, G. G. Shan, P. B. Wyatt, H. Q. Ye and W. P. Gillin, *Light: Sci. Appl.*, 2020, **9**, 32.
24 C. C. Leznoff and A. P. B. Lever, *Phthalocyanines properties and applications*, VCH, Cambridge, 1989.
25 N. Uyeda, T. Kobayashi, E. Suito, Y. Harada and M. Watanabe, *J. Appl. Phys.*, 1972, **43**, 5181–5189.
26 D. S. Lawrence and D. G. Whitten, *Photochem. Photobiol.*, 1996, **64**, 923–935.
27 C. H. Cheng, Z. Q. Fan, S. K. Yu, W. H. Jiang, X. Wang, G. T. Du, Y. C. Chang and C. Y. Ma, *Appl. Phys. Lett.*, 2006, **88**, 213505.
28 Z. Q. Fan, C. H. Cheng, S. K. Yu, K. Q. Ye, R. S. Sheng, D. C. Xia, C. Y. Ma, X. Wang, Y. C. Chang and G. T. Du, *Opt. Mater.*, 2009, **31**, 889–894.
29 S. Mori, M. Nagata, Y. Nakahata, K. Yasuta, R. Gotom, M. Kimura and M. Taya, *J. Am. Chem. Soc.*, 2010, **132**, 4054–4056.
30 D. E. J. G. J. Dolmans, D. Fukumura and R. K. Jain, *Nat. Rev. Cancer*, 2003, **3**, 380–387.
31 E. D. Anderson, A. P. Gorka and M. J. Schnermann, *Nat. Commun.*, 2016, **7**, 13378.
32 K. Yan, K. Vu, R. P. Wang and S. Madden, *Opt. Express*, 2016, **24**, 23304–23313.
33 F. Ma, S. R. Wang and X. G. Li, *J. Phys. Chem. Solids*, 2012, **73**, 589–592.
34 M. Handa, A. Suzuki, S. Shoji, K. Kasuga and K. Sogabe, *Inorg. Chim. Acta*, 1995, **230**, 41–44.

35 K. Y. Law, *Chem. Rev.*, 1993, **93**, 449–486.
36 S. Hiller, D. Schlettwein, N. R. Armstrong and D. Wöhrle, *J. Mater. Chem.*, 1998, **8**, 945–954.
37 *Organic Electronics Materials and Devices*, ed. S. Ogawa, Springer, 2015.
38 K. Han, X. Z. Lu, J. H. Xu, S. H. Ma and W. C. Wang, *Spectrosc. Spect. Anal.*, 1999, **19**, 264–267.
39 A. V. Soldatova, J. Kim, C. Rizzoli, M. E. Kenney, M. A. Rodgers, A. Rosa and G. Ricciard, *Inorg. Chem.*, 2011, **50**, 1135–1149.
40 K. Kaneto, K. Yoshino and Y. Inuishi, *J. Phys. Soc. Jpn.*, 1974, **37**, 1297–1300.
41 M. A. Baldo, D. F. O'Brien, Y. You, A. Shoustikov, S. Sibley, M. E. Thompson and S. R. Forrest, *Nature*, 1998, **395**, 151–154.
42 J. Yang, Y. Deng, Q. Wu, J. Zhou, H. Bao, Q. Li, F. Zhang, F. Li, B. Tu and D. Zhao, *Langmuir*, 2010, **26**, 8850–8856.
43 C. Lyu, H. Li, P. B. Wyatt, W. P. Gillin and H. Ye, *J. Mater. Chem. C*, 2020, **8**, 9502–9505.
44 G. te Velde, F. M. Bickelhaupt, E. J. Baerends, C. F. Guerra, S. J. A. van Gisbergen, J. G. Snijders and T. Ziegler, *J. Comput. Chem.*, 2001, **22**, 931–967.
45 J. P. Perdew, K. Burke and M. Ernzerhof, *Phys. Rev. Lett.*, 1996, **77**, 3865–3868.
46 C. Chang, M. Pelissier and P. Durand, *Phys. Scr.*, 1986, **34**, 394–404.
47 E. van Lenthe, E. J. Baerends and J. G. Snijders, *J. Chem. Phys.*, 1994, **101**, 9783–9792.
48 F. Wang and T. Ziegler, *J. Chem. Phys.*, 2005, **123**, 154102.
49 E. Runge and E. K. U. Gross, *Phys. Rev. Lett.*, 1984, **52**, 997–1000.
50 S. J. Strickler and R. A. Berg, *J. Chem. Phys.*, 1962, **37**, 814–822.